Struct Multidisc Optim (2016) 54:953–970
DOI 10.1007/s00158-016-1462-x

RESEARCH PAPER

Reliability-based design optimization of wind turbine blades for fatigue life under dynamic wind load uncertainty

Weifei Hu[1] · **K. K. Choi**[1] · **Hyunkyoo Cho**[1]

Received: 19 October 2015 / Revised: 16 February 2016 / Accepted: 8 April 2016 / Published online: 29 April 2016

Abstract This paper studies reliability-based design optimization (RBDO) of a 5-MW wind turbine blade for designing reliable as well as economical wind turbine blades. A novel dynamic wind load uncertainty model has been developed using 249 groups of wind data to consider wind load variation over a large spatiotemporal range. The probability of fatigue failure during a 20-year service life is estimated using the uncertainty model in the RBDO process and is reduced to meet a desired target reliability. Meanwhile, the cost of composite materials used in the blade is minimized by optimizing the composite laminate thicknesses of the blade. In order to obtain the RBDO optimum design efficiently, deterministic design optimization (DDO) of the 5-MW wind turbine blade is carried out first using the mean wind load obtained from the wind load uncertainty model. The RBDO is then initiated from the DDO optimum. During the RBDO iterations, fatigue hotspots for RBDO are identified among the laminate section points. For an efficient RBDO process, surrogate models of 10-min fatigue damages D_{10} at the hotspots are accurately created using the Kriging method. Using the wind load uncertainty model and surrogate models, probability of fatigue failure during a 20-year lifespan at the hotspots and the design sensitivities are calculated at given design points. Using the probability of fatigue failure and design sensitivity, RBDO of the 5-MW wind turbine blade has been successfully carried out, satisfying the target probability of failure of 2.275 %.

Keywords Wind turbine blades · RBDO · Wind load uncertainty · Reliability analysis · Fatigue life

Abbreviations

CDF	Cumulative distribution function
CoV	Coefficient of variation
DDO	Deterministic design optimization
DKG	Dynamic Kriging
DoE	Design of experiment
FE	Finite element
FORM	First-order reliability method
MCS	Monte Carlo simulation
MLE	Maximum likelihood estimation
NRMSE	Normalized root mean square error
PDF	Probability density function
RBDO	Reliability-based design optimization
SORM	Second-order reliability method
SQP	Sequential Quadratic Programming
UKG	Universal Kriging
a, $\mathbf{a}$	Shape parameter and random vector of shape parameter of Gamma distribution
b, $\mathbf{b}$	Scale parameter and random vector of scale parameter of Gamma distribution
C	Scale parameter of Weibull distribution / total cost of composite materials
$\mathbf{C}$	Random vector of scale parameter of Weibull distribution
$c_{V\Sigma}$	Copula density function for V_{10} and Σ_{10}
D_{10}	10-min fatigue damage
D_{1year}	One-year fatigue damage
D_{20year}	20-year fatigue damage
$\mathbf{d}$	Design variable vector in DDO
k, $\mathbf{k}$	Shape parameter and random vector of shape parameter of Weibull distribution

✉ K. K. Choi
kkchoi@engineering.uiowa.edu

[1] Department of Mechanical and Industrial Engineering, The University of Iowa, Iowa City, IA 52242, USA

$f_C, f_k, f_a, f_b, f_\tau$	Marginal PDF of C, k, a, b, τ
$f_{V10}, f_{I10}, f_{\Sigma 10}$	Marginal PDF of V_{10}, I_{10}, Σ_{10}
f_{VI}	Joint PDF of V_{10} and I_{10}
I_{10}, i_{10}	10-min turbulence intensity and its realization
$P_{VI}^{i,j}$	Probability of the V_{10} and I_{10} in the (i, j) cell of wind load probability table
$\overline{P}_{VI}^{i,j}$	Mean probability of the V_{10} and I_{10} in the (i, j) cell of wind load probability table
T_i	Laminate thickness random variable
V_{10}, v_{10}	10-min mean wind speed and its realization
$\mathbf{X}$	Random design vector
Σ_{10}, σ_{10}	10-min standard deviation of wind speed and its realization
τ, $\boldsymbol{\tau}$	Kendall's tau and random vector of Kendall's tau for V_{10} and Σ_{10}
$\boldsymbol{\mu}$	Random design variable vector in RBDO

1 Introduction

Wind turbine blades are the key components that drive a large wind turbine system. To reduce the levelized cost of electricity (LCOE), designing cost-effective and reliable wind turbine blades is one of the most important factors in wind turbine design. This paper proposes a reliability-based design optimization (RBDO) process for wind turbine blades considering the uncertainty of dynamic wind load and the manufacturing process. In the RBDO process, the cost of a wind turbine blade is minimized to reduce the initial investment. At the same time, target fatigue reliability is satisfied to secure continued operation and reduce the maintenance cost. For the correct RBDO process, it is essential to predict the fatigue damage over the designed lifespan of 20 years. However, accurate prediction of the fatigue damage of wind turbine blades is a challenging task because the long-term fatigue damage is uncertain due to various uncertainties from material properties, manufacturing processes, and external loads. Among those uncertainties, dynamic wind load uncertainty is the most significant source of uncertainty affecting the fatigue reliability of wind turbine blades. Thus, it is critically important to develop a wind load uncertainty model that can account for realistic uncertain wind load during the lifespan of wind turbine blades.

A simple way to consider the wind load uncertainty is by using partial safety factors (International Electrotechnical Commission 2005; Germanischer Lloyd 2010; Kong et al. 2005, 2006; Veldkamp 2008). However, the spatial and temporal wind load variation cannot be represented accurately using partial safety factors. For this reason, reliability analysis of wind turbine blades considering wind load uncertainty has been studied in the literature (Ronold et al. 1999; Ronold and Christensen 2001; Veers and Winterstein 1997; Sutherland and Veers 1995; Tarp-Johansen 2003; Hu et al. 2012). Probabilistic models for mean wind speed have been applied to characterize the annual wind load variation (Griffith and Ashwill 2011; Carta et al. 2009; Shokrieh and Rafiee 2006; Manuel et al. 2001). Measured fatigue loadings, e.g., stress and bending moments, were used to estimate wind turbine fatigue reliability (Veers and Winterstein 1997; Sutherland and Veers 1995). However, the previous studies involve only a specific probability distribution (Weibull or Rayleigh distribution) of mean wind speed to account for the frequency of fatigue damage under different wind loads. By applying a fixed Weibull distribution, only deterministic fatigue life can be obtained because the distribution is obtained based either on wind turbine standards (International Electrotechnical Commission 2005; Germanischer Lloyd 2010) or on measured wind data over 1 year at a specific location. The fixed Weibull distribution cannot truly render the wind load uncertainty over a larger spatiotemporal range, for instance at different locations and in different years. For this reason, Tarp-Johansen (Tarp-Johansen 2003) studied the statistical uncertainty of two parameters of the Weibull distribution for mean wind speed based on 1-year measurements over a period of 52 years. Besides the mean wind speed, the turbulence intensity, which represents the fluctuations in the wind speed, naturally has a significant impact on the wind load uncertainty, as the wind speed fluctuations are the source of extreme gust loads and a large part of the blade fatigue loading (Burton et al. 2011; Manwell et al. 2009). The distribution of turbulence intensity has been involved in the reliability analysis of wind turbine blades (Ronold et al. 1999; Hu et al. 2012). Additionally, one wind turbine design is often used at different wind farms. At each farm, a wind turbine is supposed to be operating for 20 years under different wind load distributions in different years. However, the wind load uncertainty at different sites and in different years cannot be represented by a single standardized load model. Thus, it is necessary to develop a wind load uncertainty model which is able to represent the realistic uncertain wind load in a large spatiotemporal range, i.e., at different sites and in different years. For this reason, a novel dynamic wind load uncertainty model is proposed in this paper. The developed joint distribution of 10-min mean wind speed V_{10} and 10-min turbulence intensity I_{10} represents wind load variation at a location in a year. The wind load variation in different years and at different locations is represented by the distributions of parameters of the joint distribution.

Few researchers have properly addressed RBDO of wind turbine blades for fatigue life under dynamic wind load uncertainty. Reliability-based design of wind turbine blades against fatigue failure was studied by Ronold et al. (Ronold et al. 1999) using a probabilistic model with measured bending moments at the blade root of a site-specific wind turbine. Toft and Sørensen (Toft and Sørensen 2011) presented a probabilistic framework for designing wind turbine blades, which requires tests with the basic composite materials and full-scale blades

during the design process. However, neither method considered the wind load uncertainty in design phases due to lack of test data. Reliability-based design of wind turbine blades against failure under extreme conditions was studied by Ronold and Larsen (Ronold and Larsen 2000) and Cheng (Cheng 2002). However, fatigue failure under wind load uncertainty was not included in their reliability-based design, either. It is more challenging to accurately and efficiently consider both wind load uncertainty and manufacturing variability in RBDO. The developed RBDO process in this paper obtains an optimal design that satisfies target fatigue reliability under the developed dynamic wind load uncertainty model and manufacturing variability.

The unique contributions of this paper include: (1) developing a dynamic wind load uncertainty model that represents realistic uncertain wind load for fatigue reliability of wind turbine systems; (2) developing a framework using RBDO techniques to design reliable and cost-effective wind turbine blades considering the developed wind load uncertainty and manufacturing variability. The main structure of the paper is provided as follows. The unique features of the developed wind turbine blade model are explained in Section 2. The novel dynamic wind load uncertainty model is provided in Section 3. Section 4 explains the methods for fatigue reliability analysis under the dynamic wind load uncertainty. Section 5 presents deterministic design optimization (DDO) formulation using the mean wind load. Section 6 presents details of random design variables, objective function, probabilistic constraints, and the RBDO formulation. Results and discussion are seen in Section 7. Finally, conclusions are given in Section 8.

2 A composite wind turbine blade model

A finite element (FE) model of a parametric composite wind turbine has been developed for fatigue analysis, DDO, reliability analysis, and RBDO. The aerodynamic properties of the blade model (e.g., airfoil type, chord length, and twist angle) are the same with the 5-MW (National Renewable Energy Laboratory) NREL reference wind turbine blade (Jonkman et al. 2009). The blade model in this paper is composed of seven parts, which are the root, forward shear web, aft shear web, leading edge, spar cap, trailing edge, and tip, as shown in Fig. 1. Each part consists of one or multiple panels. For example, the root has only one panel, while the spar cap has 14 panels. Spar cap panel 1 and spar cap panel 14 are illustrated in Fig. 1. The blade is made of 71 panels in total. The forward shear web, aft shear web, leading edge, and trailing edge consist of sandwich panels, in which composite laminates are laid at both the top and bottom surfaces and a foam core is laid in the middle. The panels in the root, spar cap, and tip are made of composite laminates (no foam core in the middle).

Composite laminates QQ1 (glass-fiber-reinforced laminate) and P2B (carbon/glass-hybrid-fiber-reinforced laminate) are selected from the Sandia National Laboratories (SNL) / Montana State University (MSU) / U.S. Department of Energy (DOE) Composite Material Fatigue Database (Mandell and Samborsky 2014), which provides material properties and fatigue testing data. In general, P2B is stronger and has better fatigue resistance than QQ1. However, P2B is much more expensive, so it tends to be used where durability is important for the performance of the blade. Gurit's Wind Turbine Blade Structural Engineering Guideline points out that carbon-fiber-reinforced laminates are currently used only on some of the largest turbines (with diameters of over about 80 m), and even then only on the spar caps (Gurit 2015). Thus, P2B is applied only on the spar cap, and QQ1 is applied on other parts in the developed blade model. A hierarchical relationship among the blade, parts, panels, and composite laminates is shown in Fig. 2. A detailed laminate schedule of the blade model is provided in the paper by Hu et al. (Hu et al. 2015). It is worth noting that the composite laminate thicknesses of QQ1 and P2B change during the optimization process (DDO and RBDO) as they are connected to the design variables in this paper.

The blade FE model consists of 3700 shell elements and 3422 nodes. Each node corresponds to multiple section points that indicate a specific location through the laminate thickness at the node. Section points associated with one node may have different materials, fibre directions, and distances from the neutral axis in laminate. Therefore, stress, fatigue damage, and the probability of fatigue failure have been studied at section points, not the nodes. The number of section points corresponding to each node depends on the number of laminate layers assigned on the corresponding shell element. As an example, shown in Fig. 3a, the node 2797 at the root is connected to a shell element that has seven layers with a stacking sequence of $\left[\pm 45/+45/\overline{-45}\right]_S$. Three section points are uniformly distributed in each layer. Therefore, there are 21 section points indicating different locations through the laminate thickness at node 2797, as shown in Fig. 3b. By using a combination of node ID and section point ID, hereafter referred to as *node-section point*, it is capable of identifying the stress, fatigue damage, and probability of fatigue failure at a specific location through the laminate thickness of the blade. In total, there are 60,954 node-section points in the blade model.

3 Dynamic wind load uncertainty model

3.1 Annual wind load variation

An annual fatigue damage can be calculated using 10-min mean wind speed and 10-min turbulence intensity factor (Hu et al. 2015). The annual fatigue damage considers 10-min

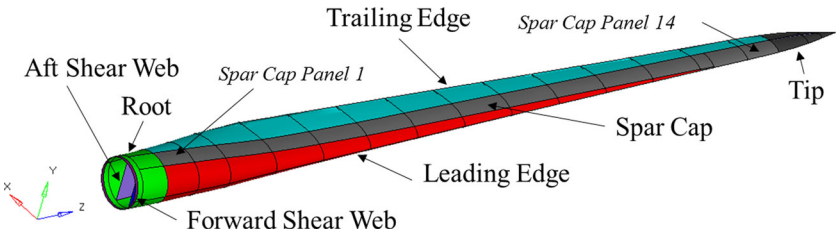

Fig. 1 Parts and panels of the composite wind turbine blade model

wind load variations in a year. However, the damage does not take account of wind load variation at different location in different years. Thus, we cannot correctly estimate fatigue reliability of a wind turbine blade at multiple locations in 20 years. Hence, in this paper, we propose a dynamic wind load uncertainty model that imposes wind load variation in a large spatiotemporal range on the aforementioned annual wind load variation.

The annual wind load variation is represented using a joint probability density function (PDF) of 10-min mean wind speed V_{10} and 10-min turbulence intensity I_{10}. There is a mathematical correlation between V_{10} and I_{10} because I_{10} is the ratio of a 10-min standard deviation of wind speed Σ_{10} to V_{10} ($I_{10} = \Sigma_{10} / V_{10}$). To exclude the mathematical correlation, the joint PDF of V_{10} and I_{10} has been derived using joint PDF of V_{10} and Σ_{10} as (Hu et al. 2015)

$$f_{VI}(v_{10}, i_{10}; C, k, a, b, \tau) = c_{V\Sigma}(v_{10}, \sigma_{10}; \tau) f_{V10}(v_{10}; C, k) f_{\Sigma 10}(\sigma_{10}; a, b) v_{10} \quad (1)$$

where f_{V10} and $f_{\Sigma 10}$ are the marginal PDFs of V_{10} and Σ_{10}, respectively. $c_{V\Sigma}$ is the copula density function for V_{10} and Σ_{10}. v_{10}, i_{10}, and σ_{10} ($\sigma_{10} = v_{10} \cdot i_{10}$) are realizations of random variables V_{10}, I_{10}, and Σ_{10}, respectively. Based on distribution fit of 249 groups of measured wind speed data, the marginal PDFs of V_{10} and Σ_{10} have been identified as Weibull distribution and Gamma distribution, respectively, using the Maximum Likelihood Estimate (MLE) method (Hu et al. 2015). The statistical correlation between V_{10} and Σ_{10} is represented using Gumbel copula, which is also the maximum likely copula type (Hu et al. 2015). The marginal PDFs of Weibull distribution for V_{10} and Gamma distribution for Σ_{10} take the forms, respectively,

$$f_{V10}(v_{10}; C, k) = \frac{k}{C}\left(\frac{v_{10}}{C}\right)^{k-1} \exp\left[-\left(\frac{v_{10}}{C}\right)^{k}\right] \quad (2)$$

$$f_{\Sigma 10}(\sigma_{10}; a, b) = \frac{1}{b^a \Gamma(a)} \sigma_{10}^{a-1} \exp\left(-\frac{\sigma_{10}}{b}\right) \quad (3)$$

where C and k are the scale parameter and shape parameter for the Weibull distribution, respectively; a and b are the shape parameter and scale parameter for the Gamma distribution, respectively; and $\Gamma(a)$ is the gamma function of a. The Gumbel copula density function $c_{V\Sigma}$ is expressed as

$$c_{V\Sigma}(u, v; \tau) = \frac{(-\ln u)^{\frac{\tau}{1-\tau}} (-\ln v)^{\frac{\tau}{1-\tau}} \left(\frac{1}{1-\tau} + w^{1-\tau} - 1\right) w^{-1-\tau} \exp(-w^{1-\tau})}{uv} \quad (4)$$

where u and v are marginal cumulative distribution function (CDF) values of V_{10} and Σ_{10}, respectively; $w = (-\ln u)^{1/(1-\tau)} + (-\ln v)^{1/(1-\tau)}$; and τ is Kendall's tau for V_{10} and Σ_{10}. By

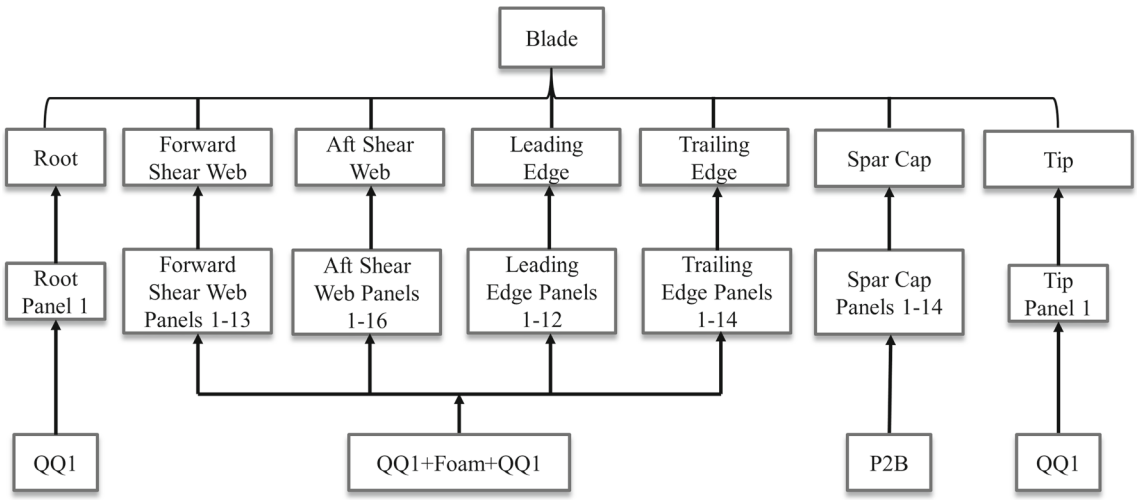

Fig. 2 Hierarchical relationship in the composite wind turbine blade model

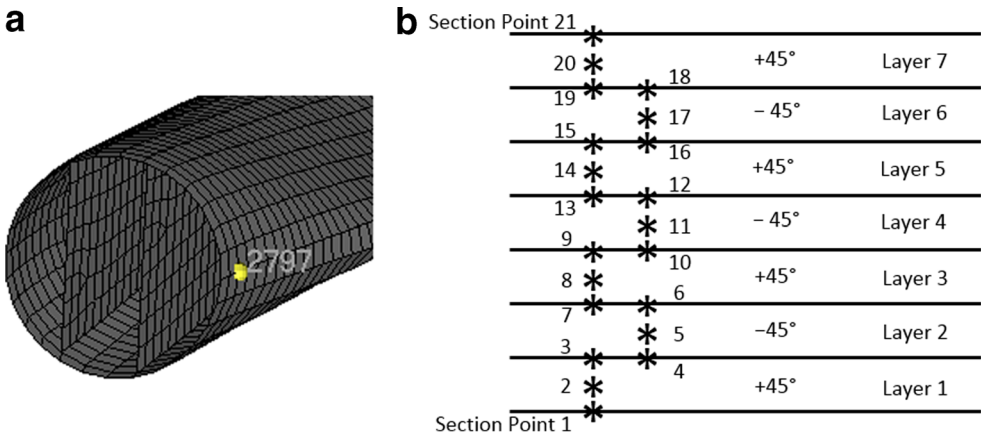

Fig. 3 **a** Node 2797; **b** Section points associated with node 2797

using the MLE method, the marginal distribution parameters C, k, a, and b, and the correlation parameter τ can be calculated based on the measured wind speed data. Substituting the calculated C, k, a, b, and τ, and Eqs. (2 - 4) into Eq. (1), a joint PDF of V_{10} and I_{10} can be obtained. The joint PDF is used to calculate the probabilities of wind conditions during 1 year, i.e., annual wind load uncertainty. The probabilities are then multiplied with the corresponding deterministic fatigue damage to calculate annual fatigue damage, as will be explained in Section 4.1.

3.2 Wind load variation in a large spatiotemporal range

The derived joint PDF of V_{10} and I_{10} is used to account for the wind load variation during 1 year at a specific location. In real situations, the wind load also varies from year to year for a specific location. In addition, the wind load is different at different locations for various reasons, e.g., the non-uniformity of the earth's surface and the thermal effect due to differences in altitude. Even though the variation of wind load in a large spatiotemporal range seems unpredictable, the distributions and correlation type of the random wind parameters, i.e., V_{10}, I_{10}, and Σ_{10}, are often assumed the same. For example, the Weibull distribution is widely used to represent the distribution of V_{10}, disregarding when or where the fatigue life prediction has been done (Burton et al. 2011; Germanischer Lloyd 2010; Griffith and Ashwill 2011; International Electrotechnical Commission 2005; Manwell et al. 2009; Ronold et al. 1999; Shokrieh and Rafiee 2006). In the same context, it is assumed that the marginal distribution types and the copula type for V_{10} and Σ_{10} do not change when dealing with wind load variation in a large spatiotemporal range in this paper. On the other hand, the joint PDF of V_{10} and Σ_{10} changes as different sets of (C, k, a, b, τ) are used. The different sets of (C, k, a, b, τ) represent wind load distributions in different years and at different locations. Hence, the novelty of the dynamic wind load uncertainty model is that the model can provide the wind load variation in a large spatiotemporal range using the distributions of C, k, a, b, and τ.

Using the 249 groups of wind data measured from different years at different locations, 249 different sets of (C, k, a, b, τ) have been calculated. Similar to the distribution fit for V_{10} and Σ_{10}, the distribution types of C, k, a, b, and τ can be identified using the same MLE method, which selects the best fit distribution according to log-likelihood function values. The computed log-likelihood function values for each candidate marginal distribution type for C, k, a, b, and τ are provided in Table 1.

As shown in Table 1, the largest log-likelihood values for C, k, a, b, and τ correspond to log-logistic, normal, generalized extreme value, Weibull, and extreme value distributions, respectively. The specific parameters for PDFs of C, k, a, b, and τ are obtained as well from the 249 sets of (C, k, a, b, τ), assuming that C, k, a, b, and τ are statistically independent. Table 2 provides the PDFs of C, k, a, b, and τ, which will be used for reliability analysis, DDO, and RBDO in Sections 4, 5, and 6, respectively.

4 Fatigue reliability analysis under wind load uncertainty

4.1 Twenty-year fatigue damage calculation

A comprehensive fatigue analysis procedure for composite wind turbine blades includes wind field simulation, aerodynamic analysis, detailed stress analysis, and fatigue damage evaluation. The procedure has been developed to calculate 10-min fatigue damage D_{10}, which is a function of random design vector $\mathbf{d}$, 10-min mean wind speed V_{10}, and 10-min turbulence intensity I_{10}, expressed as (Hu et al. 2015)

$$D_{10} = D_{10}(\mathbf{d}, V_{10}, I_{10}). \tag{5}$$

Table 1 Log-likelihood of candidate marginal distribution types for C, k, a, b, and τ

Log-likelihood	C	k	a	b	τ
Normal	−460.133	**−11.273**	−387.513	254.044	159.332
Lognormal	−453.771	−15.152	−363.056	241.609	104.754
Nakagami	−456.276	−11.859	−375.722	253.001	143.410
Rayleigh	−609.626	−276.748	−433.955	182.445	64.433
Rician	−459.954	−11.276	−385.881	254.192	158.377
Gamma	−453.967	−13.002	−368.133	248.462	127.085
Weibull	−475.839	−21.236	−389.089	**257.120**	169.065
Birnbaum-Sauuders	−454.220	−15.504	−362.710	241.967	100.490
Exponential	−768.942	−444.336	−571.864	39.0837	−82.406
Extreme Value	−506.790	−32.078	−438.082	245.713	**182.775**
Generalized Extreme Value	−453.698	−11.529	**−360.704**	256.163	179.529
Inverse Gaussian	−454.232	−15.521	−362.563	241.583	99.271
Log-logistic	**−448.182**	−12.170	−367.678	236.993	129.781
Logistic	−452.829	−12.667	−385.336	245.866	164.481

The design variable vector **d** controls the thickness of composite laminates used in the wind turbine blade. The 10-mintue fatigue damage calculation uses the superposed stress due to wind load, gravity load, and centrifugal load. The wind load is an approximated wind pressure, which is based on a potential flow solver and a rigid blade assumption, distributed on blade surface. Due to lack of wind turbine blade control, the stress due to gravity load and centrifugal load is calculated under rated rotational speed, which is 12.1 rpm. The tower shadow effect is not included due to expensive computational cost in fluid dynamics. This paper is focused on developing wind load uncertainty model and the RBDO procedure using the uncertainty model. The adoption of blade control and tower shadow effect can be studied in the future with large computational resources.

Applying the 10-min fatigue damage D_{10} in Eq. (5) and the derived joint PDF of V_{10} and I_{10} in Eq. (1), the 1-year fatigue damage D_{1year} can be calculated as

$$D_{1year}(\mathbf{d}, C, k, a, b, \tau) = 52560 \int_{V_{low}}^{V_{upp}} \int_{I_{low}}^{I_{upp}} f_{VI}(v_{10}, i_{10}; C, k, a, b, \tau) D_{10}(\mathbf{d}, v_{10}, i_{10}) \mathrm{d}v_{10} \mathrm{d}i_{10} \tag{6}$$

where "52560" indicates the number of 10-min periods in 1 year; V_{low} and V_{upp} are the lower and upper bounds of V_{10}, respectively; and I_{low} and I_{upp} are the lower and upper bounds of I_{10}, respectively. The 1-year fatigue damage in Eq. (6) cannot be explicitly expressed as a function of **d**, C, k, a, b, and τ, due to the complexity of the joint PDF and 10-min fatigue damage calculation. Thus, in practical damage calculation, the double

Table 2 Identified marginal PDFs of C, k, a, b, and τ

Parameter	Distribution type	PDF
C	Log-logistic	$f_C(x) = \frac{\exp\left[\frac{\ln(x)-2.0701}{0.1024}\right]}{0.1024x\left[1+\exp\left(\frac{\ln(x)-2.0701}{0.1024}\right)\right]^2}$
k	Normal	$f_k(x) = \frac{1}{0.2532\sqrt{2\pi}} \exp\left[\frac{-(x-2.1913)^2}{0.1282}\right]$
a	Generalized Extreme Value	$f_a(x) = 1.1888 \frac{(0.7429+0.0827x)^{-15.3746}}{exp\left[(0.7429+0.0827x)^{-14.3746}\right]}$
b	Weibull	$f_b(x) = \frac{4.1254}{0.3470}\left(\frac{x}{0.3470}\right)^{3.1254} \exp\left[-\left(\frac{x}{0.3470}\right)^{4.1254}\right]$
τ	Extreme Value	$f_\tau(x) = 0.0986^{-1} \exp\left(\frac{x-0.5696}{0.0986}\right) \exp\left[-\exp\left(\frac{x-0.5696}{0.0986}\right)\right]$

integration in Eq. (6) is numerically calculated using the Riemann integral as (Taylor 2006)

$$D_{1year}(\mathbf{d}, C, k, a, b, \tau) \approx 52560 \sum_{i=1}^{m} \sum_{j=1}^{n} P_{VI}^{i,j}(v_{10}^{i}, i_{10}^{j}; C, k, a, b, \tau) D_{10}^{i,j}(\mathbf{d}, v_{10}^{i}, i_{10}^{j}) \tag{7}$$

where m and n are the number of discrete cells in the integration domain in directions of V_{10} and I_{10}, respectively.

The probability of the V_{10} and I_{10} in the (i, j) cell can be calculated using Eq. (1) as

$$P_{VI}^{i,j}(v_{10}^{i}, i_{10}^{j}; C, k, a, b, \tau) = f_{VI}(v_{10}^{i}, i_{10}^{j}; C, k, a, b, \tau) \Delta v_{10} \Delta i_{10} \tag{8}$$

where Δv_{10} and Δi_{10} are the size of the (i, j) cell in the directions of V_{10} and I_{10}, respectively. (v_{10}^{i}, i_{10}^{j}) is the center point of the (i, j) cell. In this paper, a large range of V_{10} and I_{10} has been considered to examine the fatigue damage considering all possible wind conditions, i.e., a combination of V_{10} and I_{10}. Moriarty et al. (Moriarty et al. 2004) applied the cut-in and cut-out wind speed as the lower and upper bound, respectively, of 10-min segments in 1-year fatigue simulation, and the calculated fatigue load cycles agreed well with those obtained by a long-term extrapolation method in their work. Even though the unsteadiness when wind speed is larger than cut-out wind speed can cause large fluctuating loads, the probability of occurrence of such extreme wind conditions is very small, which makes negligible fatigue contribution in long term. Thus, the lower bound V_{low} and upper bound V_{upp} of V_{10} are set to be the cut-in wind speed of 3 m/s and cut-out wind speed of 25 m/s, respectively (Jonkman et al. 2009). The lower bound I_{low} and upper bound I_{upp} of I_{10} are set to be 0.02 and 1, respectively, so that the developed method can cover a very large range of I_{10}.

The 10-min fatigue analyses are run over the range $[V_{low}, V_{upp}]$ of V_{10} in 2 m/s increments, and the range $[I_{low}, I_{upp}]$ of I_{10} in 0.02 increments. Therefore, the number of realizations of V_{10} and I_{10} are $m = 12$ ($i = 1,\ldots,12$) and $n = 50$ ($j = 1,\ldots,50$), respectively, in Eq. (7). At each wind condition, a wind load probability is calculated using Eq. (8), and a 10-min fatigue damage is calculated using the fatigue analysis procedure developed by Hu et al. (Hu et al. 2015). In this way, a 12-by-50 wind load probability table for $P_{VI}^{i,j}$ and a 12-by-50 10-min fatigue damage table for $D_{10}^{i,j}$ can be constructed.

As an example, a wind load probability table and a 10-min fatigue damage table are illustrated using 3-D bar charts in Fig. 4a and b, respectively. In Fig. 4a, one set of (C, k, a, b, τ) ($C = 6.5856$, $k = 2.5178$, $a = 3.1570$, $b = 0.4123$, $\tau = 0.6826$), which is randomly picked from 249 sets, is used to generate the illustrated wind load probability table. Figure 4b uses 10-min fatigue damages calculated at a node-section point in the blade model. As shown in Fig. 4a, the large probabilities are concentrated at mild wind conditions, i.e., small V_{10} and I_{10}. For severe wind conditions (large V_{10} and I_{10}), the probabilities are much smaller than those corresponding to mild wind load conditions. The reason these severe wind conditions are also considered is that the 10-min fatigue damages under the severe wind conditions are much larger than those under the mild wind conditions. As shown in Fig. 4b, the 10-min fatigue damage increases exponentially as V_{10} and I_{10} increase. Hence, the severe conditions are included for the calculation of the 1-year fatigue damage.

A 3-D bar chart of the multiplication of the wind load probability table (Fig. 4a) and the 10-min fatigue damage table (Fig. 4b) is shown in Fig. 4c. As shown in Fig. 4c, in this case the distribution of the multiplication is closer to that of the wind load probability table (Fig. 4a). The large multiplication values are clustered at the mild wind conditions. The reason is that the magnitude of probability at the severe wind conditions is much smaller than that at the mild wind conditions. Therefore, we can see that the effect of mild wind conditions would dominate fatigue reliability of wind turbine blades.

Considering the wind load variation in a 20-year range and at different locations, a 20-year fatigue damage of a node-section point can be calculated as

$$\begin{aligned} D_{20year}(\mathbf{d}, \mathbf{C}, \mathbf{k}, \mathbf{a}, \mathbf{b}, \boldsymbol{\tau}) &= \sum_{t=1}^{20} D_{1year}^{t}(\mathbf{d}, C^{t}, k^{t}, a^{t}, b^{t}, \tau^{t}) \\ &= 52560 \sum_{t=1}^{20} \sum_{i=1}^{12} \sum_{j=1}^{50} P_{VI}^{i,j}(v_{10}^{i}, i_{10}^{j}; C^{t}, k^{t}, a^{t}, b^{t}, \tau^{t}) D_{10}^{i,j}(\mathbf{d}, v_{10}^{i}, i_{10}^{j}) \end{aligned} \tag{9}$$

where random vectors $\mathbf{C}$, $\mathbf{k}$, $\mathbf{a}$, $\mathbf{b}$, and $\boldsymbol{\tau}$ contain 20 sets of (C, k, a, b, τ) as $\mathbf{C} = [C^1, C^2,\ldots, C^{20}]$, $\mathbf{k} = [k^1, k^2,\ldots, k^{20}]$, $\mathbf{a} = [a^1, a^2,\ldots, a^{20}]$, $\mathbf{b} = [b^1, b^2,\ldots, b^{20}]$, and $\boldsymbol{\tau} = [\tau^1, \tau^2,\ldots, \tau^{20}]$. The 20 sets are randomly generated according to the marginal distributions in Table 2. It is noted that each set creates a different wind load probability table using Eq. (8); however, the creation is computationally efficient because Eq. (8) is analytic.

4.2 Reliability analysis using Monte Carlo simulation

The 20-year fatigue damage D_{20year} in Eq. (9) is random because the laminate thicknesses are random due to manufacturing variability, and the random vectors $\mathbf{C}$, $\mathbf{k}$, $\mathbf{a}$, $\mathbf{b}$, and $\boldsymbol{\tau}$ are random due to wind load uncertainty. Consequently, a fatigue failure ($D_{20year} > 1$) in 20 years should be measured with its probability, not with its one realization (deterministic value). The probability of fatigue failure cannot be calculated using a sensitivity-based reliability method such as the first-order reliability method (FORM) (Ditlevsen and Madsen 1996;

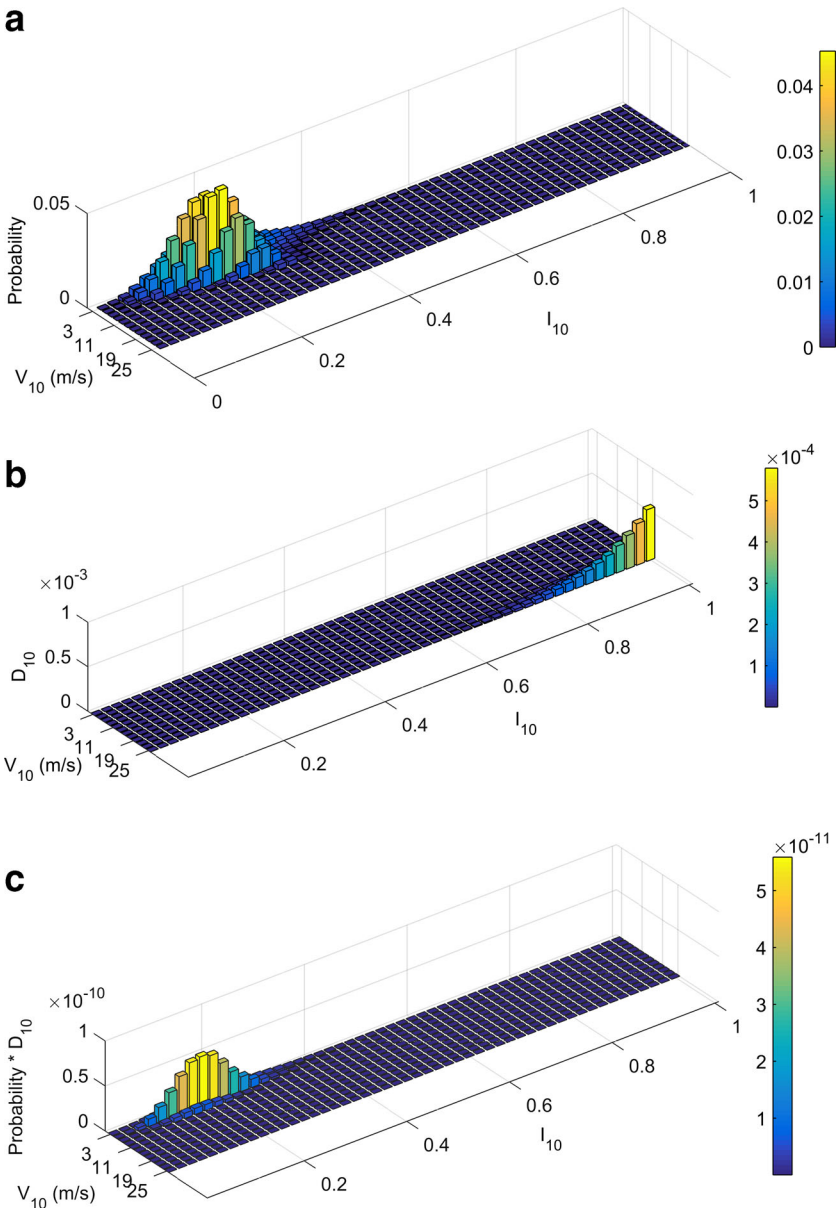

Fig. 4 Three-dimensional bar chart of: **a** wind load probability table; **b** 10-min fatigue damage table; **c** multiplication of the wind load probability table and the 10-min fatigue damage table

Haldar and Mahadevan 2000) or the second-order reliability method (SORM) (Hohenbichler and Rackwitz 1988) because the sensitivity (gradient) of D_{20year} in Eq. (9) cannot be readily obtained due to its implicit feature. Thus, in this paper, the probability of fatigue failure is calculated using a sampling-based reliability method that uses Monte Carlo simulation (MCS). Using Eq. (9) and MCS, the probability of fatigue failure of a node-section point is calculated as

$$\begin{aligned} P(\text{Fatigue Life} < 20 \text{ years}) &= P\left(D_{20year}(\mathbf{Y}) > 1\right) \\ &= \int_{D_{20year}(\mathbf{Y})>1} f_{\mathbf{Y}}(\mathbf{y})d\mathbf{y} \\ &= \int_{\mathbb{R}^N} I_{\Omega_F}(\mathbf{y}) f_{\mathbf{Y}}(\mathbf{y})d\mathbf{y} \cong \frac{1}{NMCS}\sum_{i=1}^{NMCS} I_{\Omega_F}\left[\mathbf{y}^{(i)}\right] \end{aligned} \tag{10}$$

where $\mathbf{Y} = [\mathbf{X}, \mathbf{C}, \mathbf{k}, \mathbf{a}, \mathbf{b}, \boldsymbol{\tau}]$, $\mathbf{y}^{(i)}$ is the i^{th} realization of $\mathbf{Y}$, and $f_{\mathbf{Y}}(\mathbf{y})$ is the PDF of $\mathbf{Y}$. It is assumed that all the random variables in $\mathbf{Y}$ are independent. Thus, the realization $\mathbf{y}^{(i)}$ is randomly generated based on the PDF of a random design vector $\mathbf{X}$ and the PDFs of random parameters (C, k, a, b, τ) in the wind load uncertainty model.

In reliability analysis and RBDO, the random design vector $\mathbf{X}$ replaces the design variable vector $\mathbf{d}$ in order to consider the design uncertainty (manufacturing variability). The mean of the random design vector $\mathbf{X}$ is the design variable vector $\boldsymbol{\mu}$ in RBDO. Each realization $\mathbf{y}^{(i)}$ includes 20 sets of (C, k, a, b, τ), which represent the wind load variation in 20 years. *NMCS* is the number of realizations for MCS. Ω_F is the failure domain such

that $D_{20year}(\mathbf{Y})>1$, and I_{Ω_F} is an indicator function defined as

$$I_{\Omega_F}(\mathbf{y}) = \begin{cases} 1, & \text{for } \mathbf{y}\in\Omega_F \\ 0, & \text{otherwise} \end{cases} \quad (11)$$

The probability of failure in Eq. (10) will be used as probabilistic constraints in the RBDO process. In this way, the uncertainty of wind load and manufacturing variability can be considered in the design optimization process. Therefore, a reliable as well as cost-effective optimum design can be obtained.

5 Deterministic design optimization

5.1 Mean wind load generation

A deterministic design optimization (DDO) procedure has been carried out for the composite wind turbine blade before RBDO. The purpose of DDO is to obtain a DDO optimum design, which usually provides a good initial design for RBDO, so that less computational effort will be required in the following RBDO procedure. In addition, DDO does not involve the dynamic wind load uncertainty. Thus, a representative wind load, which accounts for a mean wind load effect on 20-year fatigue damage, needs to be used in DDO. This representative wind load is provided by using a mean wind load probability table that is generated using the Monte Carlo simulation (MCS) method. The procedure to calculate the mean wind load probability table is explained below.

(1) Generate one million MCS sample sets of (C, k, a, b, τ) based on the identified distributions in Table 2.
(2) Create one million wind load probability tables. The probability value $P_{VI}^{i,j}$ in each cell (corresponding to each combination of v_{10}^i and i_{10}^j) in the probability table is calculated using Eq. (8).
(3) Calculate an average value $\overline{P}_{VI}^{i,j}$ of one million probability values corresponding to the same wind condition v_{10}^i and i_{10}^j. Repeat for all wind conditions.

The generated mean wind load probability table is schematically shown in Fig. 5. Each cell in the mean wind load probability table contains an averaged probability of one wind load considering the wind load variation in a large spatiotemporal range.

5.2 Design variables

The design variables control the thicknesses of the composite laminates. The thicknesses of laminates in the same panel are assumed identical. In order to reduce the number of design variables, one design variable is linked to laminate thickness in one or multiple panels. For example, design variable 1 is linked to laminate thickness in the root panel; design variable 2 is linked to laminate thickness in panels 1 to 5 of the forward shear web. The detailed linkage between design variables and linked panels is shown in Table 3. The initial value, lower and upper bounds of design variables, and corresponding composite materials are also listed in Table 3. It is noted that a design variable is not the total thickness of the corresponding panels. It is the thickness of one composite laminate. For example, when design variable d_1 is 4 mm, the thickness of root panel is 28 mm because there are seven laminate layers in the root panel (Hu et al. 2015).

5.3 Objective function

The normalized total cost of composite materials that are used in the blade is set as the objective function, which is expressed as

$$C(\mathbf{d}) = \left(4.18\times 1000\times \sum_{i}^{11} m_i^0 \frac{d_i}{d_i^0} + 11.70\times 1000\times m_{12}^0 \frac{d_{12}}{d_{12}^0}\right)/Cost^0 \quad (12)$$

where the design variable vector $\mathbf{d}=[d_1, d_2,\ldots, d_{12}]$; m_i^0 (unit: ton) is the initial mass of panel(s) linked to the i^{th} design variable; d_i^0 (unit: mm) is the initial value of design variable (Table 3); and $Cost^0$ is the total cost of composite materials at the initial design. By dividing current cost value by $Cost^0$ in Eq. (12), the objective function is normalized to match its significance with fatigue constraints in the DDO process. According to TPI Composites (TPI Composites 2003), the material costs of QQ1 (d_1 to d_{11}) and P2B (d_{12}) are \$4.18/kg and \$11.70/kg, respectively. Therefore, the cost of the carbon/glass-hybrid-fiber-reinforced laminate P2B is 2.8 times more than that of QQ1, which is a glass-fiber-reinforced laminate.

5.4 Fatigue constraints

The constraints for DDO are to satisfy the 20-year fatigue lifespan. In other words, the 20-year fatigue damages for all node-section points in the blade model should be smaller than 1. Under the assumption that the mean wind load condition continues for 20 years, the 20-year fatigue damage is calculated as

$$D_{20year}(\mathbf{d}) = 52560\times 20 \times \sum_{i}^{12}\sum_{j}^{50} \overline{P}_{VI}^{i,j}\left(v_{10}^i, i_{10}^j\right) D_{10}^{i,j}\left(\mathbf{d}, v_{10}^i, i_{10}^j\right) \quad (13)$$

where 52560 indicates the number of 10-min periods in 1 year; 20 indicates that the designed lifespan is 20 years;

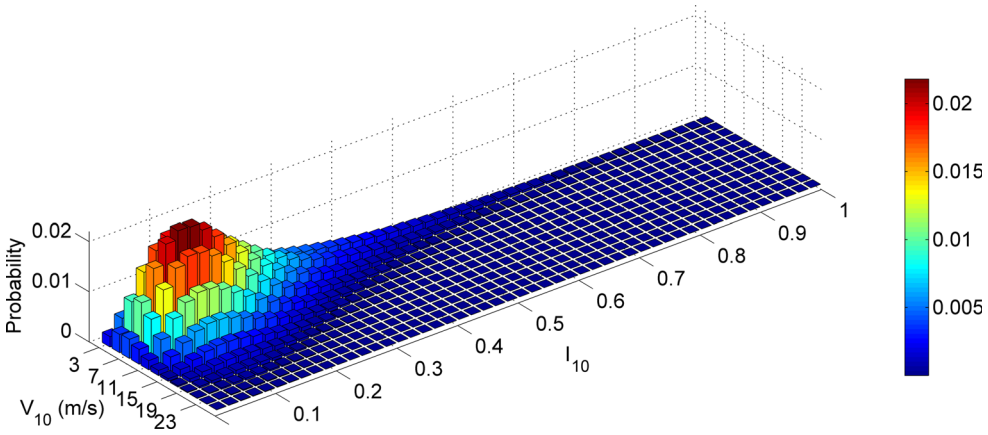

Fig. 5 Three-dimensional bar chart of the mean wind load probability table

and $\overline{P}_{VI}^{i,j}$ (v_{10}^i, i_{10}^j) is the mean probability value corresponding to the wind condition $V_{10} = v_{10}^i$ and $I_{10} = i_{10}^j$, as obtained in Section 5.1.

The fatigue hotspots are the node-section points where fatigue is considered as the DDO constraints. The selection of fatigue hotspots is a challenging issue due to the complexity of the blade model. It is quite demanding computationally to check the fatigue damages of all the 60,954 node-section points during the DDO procedure. In addition, the fatigue-critical node-section points may vary in each DDO iteration due to design change. Thus, the fatigue hotspots need to be selected wisely in order to save computational time and to make sure that all node-section points satisfy the 20-year fatigue life constraints at the DDO optimum design. The brief procedure of hotspot selection in DDO is explained below.

(1) Calculate 20-year fatigue damages of all node-section points of the blade at the initial design.
(2) For each panel, find the node-section point that has the largest fatigue damage in the panel. These node-section points with largest fatigue damages are the initial hotspots in DDO.
(3) Launch the DDO procedure.
(4) After five iterations, stop the DDO procedure. Check all the node-section points at the latest design, add new hotspots, and go to step 3. If the DDO procedure is converged under five iterations, go to step 5.
(5) Check the 20-year fatigue damages of all the node-section points at the converged design. If there is no new hotspot, DDO is converged. If there are new hotspots, add them and go to step 4.

In conclusion, the DDO of the blade for fatigue under the mean wind load can be formulated as

$$\begin{aligned} &\text{minimize } C(\mathbf{d}) \\ &\text{subject to } G_k(\mathbf{d}) = D_{20year}^k(\mathbf{d}) - 1 \le 0,\ k = 1, 2, \ldots, NC \\ &\qquad \mathbf{d}^L \le \mathbf{d} \le \mathbf{d}^U, \mathbf{d} \in \mathbb{R}^{NDV} \end{aligned} \tag{14}$$

where $\mathbf{d}$ is the 12-dimensional design variable vector for laminate thicknesses; $\mathbf{d}^L$ and $\mathbf{d}^U$ are the lower bound and upper

Table 3 Initial value, lower and upper bounds of DDO design variables, linked panels, and composite materials

Design variable	Initial value (mm)	Lower Bound (mm)	Upper Bound (mm)	Linked panel	Composite material
d_1	4	2	8	Root Panel 1	QQ1
d_2	4	2	16	Forward Shear Panels 1-5	QQ1
d_3	4	2	16	Forward Shear Panels 6-9	QQ1
d_4	4	2	16	Forward Shear Panels 10-13	QQ1
d_5	4	2	16	Aft Shear Web Panels 1-4	QQ1
d_6	4	2	16	Aft Shear Web Panels 5-8	QQ1
d_7	4	2	16	Aft Shear Web Panels 9-12	QQ1
d_8	4	2	16	Aft Shear Web Panels 13-16	QQ1
d_9	4	2	8	Tip Panel 1	QQ1
d_{10}	4	2	8	Leading Edge Panels 1-12	QQ1
d_{11}	4	2	8	Trailing Edge Panels 1-14	QQ1
d_{12}	2.5	1.5	4.5	Spar Cap Panels 1-14	P2B

bound for the design variable vector, respectively (Table 3); G_k is the k-th constraint function, which includes 20-year fatigue damage of the k-th hotspot; and NC is the number of constraints, i.e., number of hotspots. After DDO, the obtained DDO optimum design is used as the initial design for RBDO, as explained in Section 6. The DDO results are discussed in Section 7.

6 Reliability-based design optimization

6.1 Random design variables

In RBDO, the uncertainty of composite laminate thickness due to the manufacturing process has been considered in addition to the developed dynamic wind load uncertainty. Reliability-based design optimization requires evaluation of fatigue reliability to consider these uncertainties. An accurate evaluation of the fatigue reliability requires much more computational cost than deterministic 20-year fatigue damage for DDO. Due to the curse of dimensionality, RBDO problem with over than 10 dimension is very difficult to carry out. In addition, the random parameters C, k, a, b and τ also take dimensions in the RBDO problem. Therefore, the number of design variables is reduced to seven in this paper. It is noted that the wind load uncertainty is fully considered by using all the random parameters C, k, a, b and τ. The RBDO process may not produce the most economical design; however, it will produce a reliable and cost effective design using the seven design variables. Before explaining the reduced design variables, three assumptions are introduced for the uncertainty of laminate thickness.

(1) The composite laminate thickness is assumed to follow normal distribution.
(2) The coefficient of variation (CoV) of the laminate thickness is assumed the same at different designs. Therefore, standard deviation of the laminate thickness changes linearly as design (nominal or mean thickness) changes.
(3) The randomness of laminate thickness corresponding to seven design variables in seven parts (Section 2) is assumed independent. Thus, the laminate thicknesses in seven parts are represented by seven independent random variables, respectively.

To reduce 12 design variables in DDO to seven design variables in RBDO, a transformation is required. Let T_i, $i=1, 2, \ldots, 12$, be laminate thickness random variables corresponding to the twelve design variables d_i used in DDO. Let X_j, $j=1, 2, \ldots, 7$, be independent random variables used in RBDO. Each random variable corresponds to a laminate thickness in one part of the blade model (Fig. 2). A linear relationship, which is used to link an RBDO random variable to laminate thickness random variable(s), is expressed as

$$T_i = \begin{cases} d_1^{DDO} X_1 & \\ d_i^{DDO} X_2 & \text{for } i = 2, 3, 4 \\ d_i^{DDO} X_3 & \text{for } i = 5, 6, 7, 8 \\ d_i^{DDO} X_{i-5} & \text{for } i = 9, 10, 11, 12 \end{cases} \tag{15}$$

where d_i^{DDO} is the ith design variable at DDO optimum. Because the relationship between T_i and X_j is linear, the CoV of X_j (c_{X_j}) is equal to the corresponding CoV of T_i. In addition, c_{X_j} is constant due to assumption (2). By referring to SNL/MSU/DOE Composite Material Fatigue Database (Mandell and Samborsky 2014), it is obtained that the CoV of QQ1 and P2B are $c^{\mathrm{QQ1}}=0.0323$ and $c^{\mathrm{P2B}}=0.0203$, respectively. Thus, $c_{X_j} = c^{\mathrm{QQ1}}=0.0323$ for $j=1, 2, \ldots, 6$, and $c_{X_7} = c^{\mathrm{P2B}}=0.0203$.

In order to distinguish the DDO design variable $\mathbf{d}$, the Greek letter $\boldsymbol{\mu}$, which represents the mean of random variable $\mathbf{X}$, is used as the random design variable in RBDO. The properties of random design variables for RBDO are summarized in Table 4, where $\boldsymbol{\mu}^L$, $\boldsymbol{\mu}^0$, and $\boldsymbol{\mu}^U$ are the lower bound, initial, and upper bound of the random design variables, respectively. The initial design variables are all equal to 1, so that the DDO optimum design is used as the initial design for RBDO by Eq. (15). The lower bound and upper bound of random design variables are obtained by dividing the lower bound and upper bound, respectively, of laminate thickness (T_i in Eq. (15)) by the DDO optimum design.

6.2 Objective function

Similar to the DDO process, the normalized total cost of composite materials is set as the objective function, which is expressed as

$$C(\boldsymbol{\mu}) = \left(4.18 \times 1000 \times \sum_{i}^{6} M_i^0 \frac{\mu_i}{\mu_i^0} + 11.70 \times 1000 \times M_7^0 \frac{\mu_7}{\mu_7^0}\right) / Cost^{DDO} \tag{16}$$

where M_i^0 (unit: ton) is the mass of the ith part at the RBDO initial design, i.e., the DDO optimum design; μ_i^0 is the RBDO initial design corresponding to the ith part; μ_i is the current design corresponding to the ith part; $i=1, 2, \ldots, 7$; and $Cost^{DDO}$ is the total cost of composite materials at the DDO optimum design, which is obtained in DDO. It is noted that the cost is normalized at DDO optimum design because it is the initial design of RBDO. Hence, the objective function is normalized to

Table 4 Properties of random design variables

Random design variable	Distribution	μ^L	μ^0	μ^U	CoV	Corresponding part	Composite laminate
μ_1	Normal	0.5010	1	2.0039	0.0323	Root	QQ1
μ_2	Normal	0.5707	1	1.7988	0.0323	Forward Shear Web	QQ1
μ_3	Normal	1.0000	1	1.8184	0.0323	Aft Shear Web	QQ1
μ_4	Normal	1.0000	1	4.0000	0.0323	Tip	QQ1
μ_5	Normal	0.4230	1	1.6919	0.0323	Leading Edge	QQ1
μ_6	Normal	0.3764	1	1.5057	0.0323	Trailing Edge	QQ1
μ_7	Normal	0.3898	1	1.1695	0.0203	Spar Cap	P2B

match its significance with probabilistic constraints in the RBDO process.

6.3 Probabilistic constraints

The probability of fatigue failure has been obtained in Eq. (10). The probabilistic constraint in RBDO is the probability of fatigue failure (fatigue life smaller than 20 years) at hotspots being smaller than a target probability of failure. Its normalized form can be represented using Eq. (10) as

$$Q_j(\mathbf{Y}) = \frac{P\left(D^j_{20year}(\mathbf{Y}) > 1\right)}{P^{\text{tar}}_{F_j}} - 1 \le 0,\ j = 1, \ldots, NC \qquad (17)$$

where $P^{tar}_{F_j}$ = 2.275 % is the target probability of failure for the jth probabilistic constraint; NC is the number of probabilistic constraints (i.e., number of hotspots). In literatures, target probability of failure are lower than 2.275 %, such as 1.1×10^{-3} and 4.2×10^{-3}, for a blade failure in 20 years (Veldkamp 2008; Rademakers et al. 2002). However, the low target values could only be achieved using the standardized wind load model, which does not consider the wind load uncertainty in large spatiotemporal range. In reality, about 0.023 blades per wind turbine have been changed in a year averagely (Echavarria et al. 2008; Institut für Solare Energieversorgungstechnik 2006). Because a more realistic wind load uncertainty model is applied in this paper, the authors use a reasonable target value of 2.275 % for 20-year fatigue life, which is used in many engineering applications.

The hotspots for RBDO are the node-section points of which the probability of fatigue failure can represent the probability of fatigue failure of the whole wind turbine blade. By using enough hotspots, the RBDO optimum design could guarantee that all the node-section points in the blade design satisfy the 2.275 % target probability of failure. However, too many hotspots would increase the computational cost because it is expensive to create accurate surrogate models for calculating 20-year fatigue damage at each hotspot. To resolve this dilemma, three hotspot-selection criteria have been developed as briefly explained below.

(1) Select the node-section points, which correspond to active DDO constraints at the DDO optimum design, as hotspots for RBDO.
(2) In each part, select the node-section point, which has the maximum 1-year fatigue damage as a hotspot for RBDO. The 1-year fatigue damage is calculated by using Eq. (7) and replacing $P^{i,j}_{VI}$ with the mean wind load probability $\overline{P}^{i,j}_{VI}$.
(3) For each part, select the node-section point, which has the maximum 1-year fatigue damage among all node-section points inside and adjacent to the part, as a hotspot for RBDO.

The adjacent node-section points are in the other parts, but they share nodes with the part currently being checked. As demonstrated in Fig. 6, the node-section point a is inside part A, while the node-section point b is in part B and adjacent to part A. Therefore, node-section points inside the dashed-dotted line of Fig. 6 are checked by criterion (2), while node section points inside the dotted line are checked by criterion (3). Criterion (3) is included because a design change in one part will affect not only the fatigue damage of node-section points inside the part but also the fatigue damage of node-section points adjacent to the part.

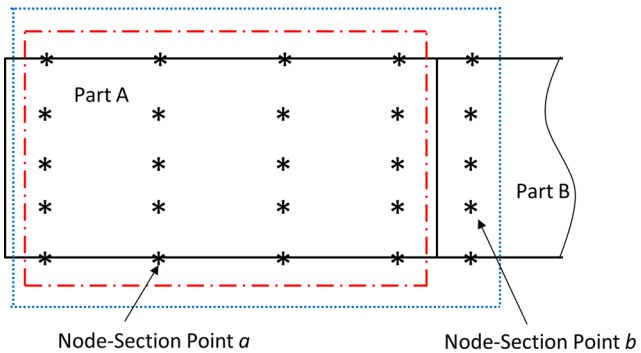

Fig. 6 Demonstration of inside node-section points and adjacent node-section points for selecting RBDO hotspots

By using the hotspot-selection criteria, nine hotspots are selected at the RBDO initial design. The nodal locations of the nine hotspots are shown in Fig. 7. It is worth noting that the hotspots may move to different locations as the RBDO iteration proceeds. In order to include all the hotspots for RBDO, the hotspots are re-checked every four RBDO iterations. If new hotspots based on the three criteria are found, the newfound hotspots are included for probabilistic constraints. If no new hotspot is found, the RBDO iteration is continued using the previously found hotspots.

When hotspots are identified, the probability of fatigue failure in Eq. (10) should be calculated at the hotspots. To obtain the probability of fatigue failure accurately and efficiently, the 20-year fatigue damage in Eq. (9) needs to be accurately and efficiently calculated. In the RBDO process, surrogate model methods are frequently used to achieve accuracy as well as efficiency. In this paper, two types of surrogate models have been created to investigate the efficiency and accuracy of 20-year fatigue damage calculation. The first type is the surrogate model of 1-year fatigue damage $D_{1year}(\mathbf{X}, C, k, a, b, \tau)$ (replace **d** by **X** in Eq. (7)), which is a function of 12 random variables: seven random design variables and five random parameters of (C, k, a, b, τ). The second type is the surrogate model of the 10-min fatigue damage $D_{10}(\mathbf{X})$ (replace **d** by **X** in Eq. (5)) given V_{10} and I_{10}, which is a function of seven random design variables. To calculate 20-year fatigue damage for each selected hotspot, it only needs one surrogate model of 1-year fatigue damage. However, the 1-year fatigue damage has 12 dimensions and is highly nonlinear. On the other side, the 10-min fatigue damage has only seven dimensions and is mildly nonlinear. However, it needs 600 ($12 \times 50 = 600$) surrogate models for 10-min fatigue damage D_{10} (one surrogate model for one cell in the 10-min fatigue damage table) to calculate 20-year fatigue damage for each selected hotspot. In order to decide which type of surrogate model is more accurate and efficient, the following study has been carried out.

For the first case, the Universal Kriging (UKG) method (Kyriakidis and Goodchild 2006; Zhao et al. 2011) with 1350 design of experiment (DoE) samples is used to generate nine (number of hotspots) surrogate models for 1-year fatigue damage on a 3-sigma local window (a hypercube centered at the current design, each side of which has ±3 standard deviations). For the second case, the same (UKG) method with 150 DoE samples is used to generate $600 \times 9 = 5400$ D_{10} surrogate models on the same 3-sigma local window. The reason that 1350 DoE samples is used for the first case, while only 150 DoE samples are used for the second case, is because the responses of the first case is much more nonlinear than the responses of the second case. On the other hand, the second case requires generating 5400 surrogate models compared to the first case, which require generating nine surrogate models. Both cases have run on the same Linux server (72 GB of RAM, 12 cores, 2.9 GHz Intel CPU). The computational times for generating nine D_{1year} surrogate models with 1350 DoE samples and 5400 D_{10} surrogate models with 150 DoE samples are about 37 and 26 hours, respectively. Therefore, using D_{10} surrogate models is more efficient.

The accuracy of the surrogate models at the RBDO initial design is checked by calculating the normalized root mean square error (NRMSE) of 20-year fatigue damage using 1000 testing samples. The NRMSE is calculated as

$$\mathrm{NRMSE} = \frac{\sqrt{\sum_{i}^{1000}\left(D^{i}_{20year} - \hat{D}^{i}_{20year}\right)^{2}/1000}}{\max\left(D_{20year}\right) - \min\left(D_{20year}\right)} \tag{18}$$

where D^{i}_{20year} is the 20-year fatigue damage at the ith testing sample by using 20-year fatigue damage calculation procedure (Section 4.1); $\hat{D}^{i}_{20year}$ is the 20-year fatigue damage at the ith testing sample by using surrogate models; $\max(D_{20year})$ is the maximum of 20-year fatigue damages among all D^{i}_{20year}; and $\min(D_{20year})$ is the minimum of 20-year fatigue damages among all D^{i}_{20year}, $i = 1, 2, \ldots, 1000$. The maximum NRMSE using D_{10} surrogate models is 5.792E−4 at the third hotspot, while the minimum NRMSE using D_{1year} surrogate models is 9.452E−3. Therefore, it shows that using the D_{10} surrogates is more accurate as well as more efficient. In addition, the maximum NRMSE of the D_{10} surrogate models is smaller than 1E−3, which indicates the D_{10} surrogate models are accurate enough for RBDO. Thus, D_{10} surrogate models using UKG are employed for the RBDO process in this paper. As the RBDO iteration proceeds, new sets of D_{10} local surrogate models are created. The accuracy of the new sets of D_{10} surrogate models is not checked in order to save computation time. However, the accuracy of D_{10} surrogate models is checked at the final RBDO optimum design using NRMSE.

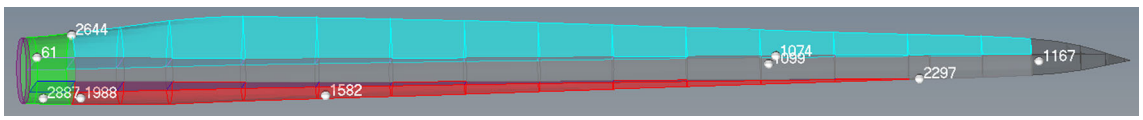

Fig. 7 Nodal locations of the nine hotspots at the RBDO initial design

6.4 RBDO formulation and flowchart

The RBDO problem can be formulated as

$$\begin{aligned} &\text{minimize } C(\boldsymbol{\mu}) \\ &\text{subject to } Q_j(\mathbf{Y}) \le 0, j = 1, \ldots, NC \\ &\qquad \boldsymbol{\mu}^L \le \boldsymbol{\mu} \le \boldsymbol{\mu}^U, \boldsymbol{\mu} \in \mathbb{R}^7 \text{ and } \mathbf{Y} \in \mathbb{R}^{107} \end{aligned} \tag{19}$$

where $\mathbf{Y}$ is the 107-dimensional random vector including seven random design variables and 20 sets of (C, k, a, b, τ); $\boldsymbol{\mu}$ is the 7-dimensional design variable vector; $C(\boldsymbol{\mu})$ is the normalized cost as shown in Eq. (16); and the normalized constraints in Eq. (19) are from Eq. (17). In this paper, Matlab's Sequential Quadratic Programming (SQP) algorithm (Matlab 2012a 2012) is used for the RBDO optimizer.

As explained in Section 6.1, the coefficient of variation (CoV) of each random design variable is constant in the RBDO process. In this paper, RBDO with constant CoV of random variable, which has been developed by Cho et al. (Cho et al. 2016), is applied to solve the RBDO problem. A flowchart of the RBDO process is shown in Fig. 8. The basic steps to carry out the RBDO process including hotspot selection and surrogate model creation are listed below.

(1) Check hotspots at the RBDO initial design.
(2) Create (600 × No. of hotspots) surrogate models of 10-min fatigue damage (D_{10}) on the 3-sigma local window. The D_{10} surrogate models are used to calculate 20-year fatigue damage (D_{20year}) in Eq. (9).
(3) Launch the SQP algorithm.
(4) For each design iteration or line search, create the local D_{10} surrogate models at the hotspots.
(5) After four design iterations, check hotspots at the current design. If there are new hotspots, add their probability of fatigue failure to the probabilistic constraints and go to step 3. If the RBDO procedure is converged under four iterations, go to step 6.
(6) Check the hotspots at the converged design. If there are new hotspots, add their probability of fatigue failure to the probabilistic constraints and go to step 3. If there is no new hotspot, RBDO optimum design is obtained.

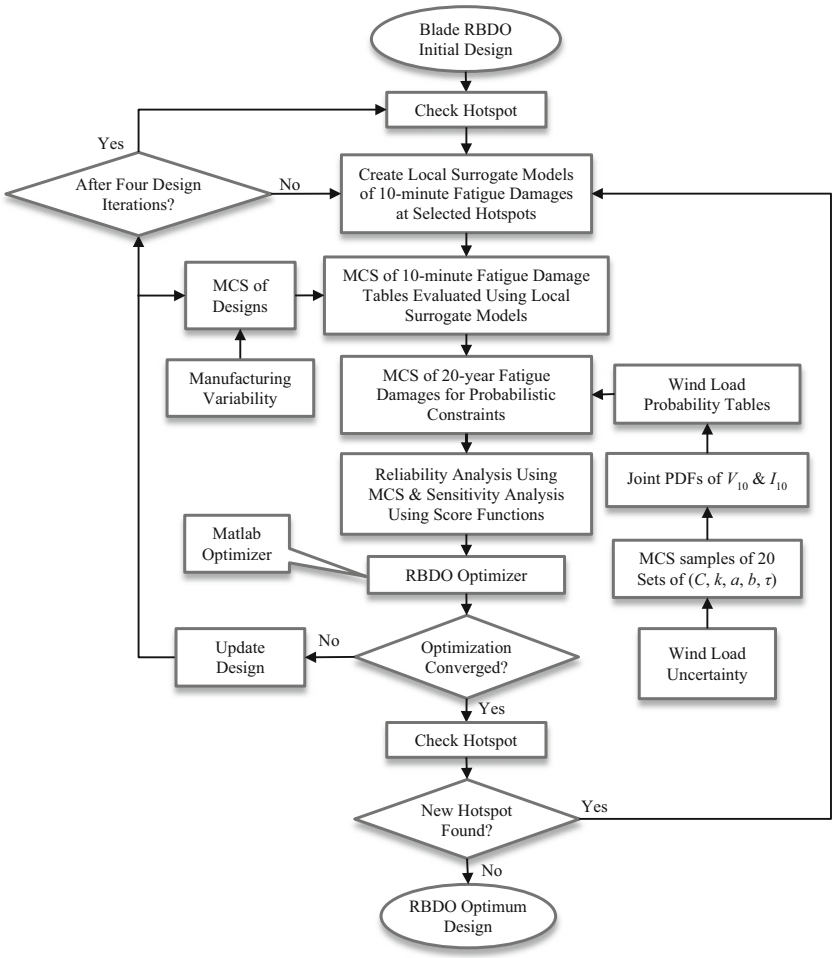

Fig. 8 Flowchart of the RBDO process

7 Results and discussion

The DDO process has been carried out on a Linux machine (Dell PowerEdge R720 single server, 8 quad-core Xeon E5-2690 CPUs-32 cores, 2.9 GHz, 256 GB of RAM). Fifteen cores are used in parallel. The DDO process consists of 35 design iterations. The DDO procedure is converged after 35 design iterations as the design change is less than the tolerance 1E−3 and the relative maximum constraint violation is less than the same tolerance. The number of hotspots is increased from 69 at the initial design to 120 at the DDO optimum design. The total computational time for the entire DDO process is about 152 hours (6.3 days).

Table 5 compares the design variables, objective function, and fatigue life of the blade at the initial design and the DDO optimum design. Here, the fatigue life (unit: year) of the blade is calculated as 20 dividing the maximum 20-year fatigue damage among all node-section points in the blade model. As shown in Table 5, the fatigue life of the initial design is only 0.0004 year, which obviously does not satisfy the target fatigue lifespan of 20 years. After the DDO procedure, the cost is increased by 31.53 % and the fatigue life of the blade model is significantly increased to satisfy the 20-year fatigue lifespan.

The optimization histories of the cost function and fatigue life are plotted in Fig. 9. As shown in Fig. 9, there is a drop at the 10th iteration in the fatigue life history. The drop occurs because new fatigue hotspots are identified after 10 design iterations. Among the new hotspots, one hotspot has significantly large fatigue damage compared to the others. Hence, incorporating this new hotspot reduces the fatigue life while the cost remains the same. After 35 iterations, the DDO procedure is converged and no new hotspots are found.

Table 5 Design variables, cost, mass, and fatigue life at initial design and at DDO optimum design

	Initial design	DDO optimum design
d_1 (mm)	4	3.99
d_2 (mm)	4	3.50
d_3 (mm)	4	4.45
d_4 (mm)	4	**6.51**
d_5 (mm)	4	2.00
d_6 (mm)	4	2.00
d_7 (mm)	4	**7.06**
d_8 (mm)	4	4.40
d_9 (mm)	4	2.00
d_{10} (mm)	4	4.73
d_{11} (mm)	4	5.31
d_{12} (mm)	2.5	3.85
Normalized Cost	1	1.3153
True Cost ($)	9549.42	125605.49
Mass (ton)	18.4984	21.8050
Fatigue Life (year)	0.0004	19.9995

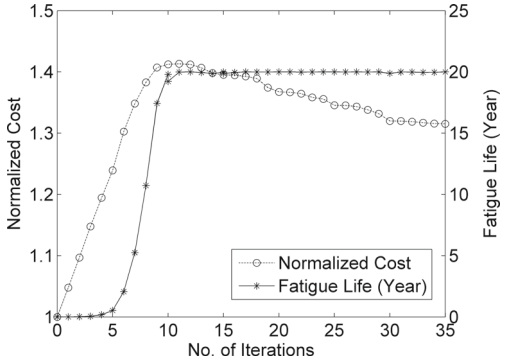

Fig. 9 Histories of normalized cost and fatigue life in DDO

The RBDO process has been carried out on the same machine used for DDO using fifteen cores in parallel. The entire RBDO process is converged using 12 design iterations, 12 additional line searches, and 4 episodes of hotspot checking. Each design iteration or line search requires one set of D_{10} surrogate models and one fatigue reliability analysis. Thus, 25 sets of D_{10} surrogate models have been generated, including one set for the RBDO initial design. Accordingly, there are 25 fatigue reliability analyses for the RBDO initial design, designs at 12 iterations, and additional 12 line searches. At each iteration, 200000 MCS of 20 sets of (C, k, a, b, τ) are used to calculate the probabilities of fatigue failure and design sensitivities of the probabilistic constraints. It takes about 16 hours to generate one set of local surrogate models and three hours for 1 fatigue reliability analysis. The computational time is about fifteen hours for checking hotspots at a design. The total computational time for the entire RBDO process is about 535 hours (22.3 days). In order to reduce the computational time, the authors has proposed methods, for example, efficient hotspot selection for RBDO and surrogate model generation for 10-min fatigue damage as explained in Section 6.3. The proposed RBDO method also depends on computational resources. If a high-performance computer, which has more cores than the Linux machine, is used, the total computational time can be reduced further.

At the RBDO initial design, nine hotspots are identified as explained in Section 6.3. Since each RBDO constraint (probability of fatigue failure at each hotspot) requires 600 local D_{10} surrogate models, 5400 local D_{10} surrogate models are created at each RBDO iteration or line search. There are 150 DoE samples used to create one set of 5400 local D_{10} surrogate models. At a new design iteration or line search design point, previously used DoE samples that are inside the new local window are re-used to create local D_{10} surrogate models in the new local window. At the fourth RBDO iteration, a new hotspot has been found, which is node 2657 - section point 15. All the previous selected nine hotspots are kept as probabilistic

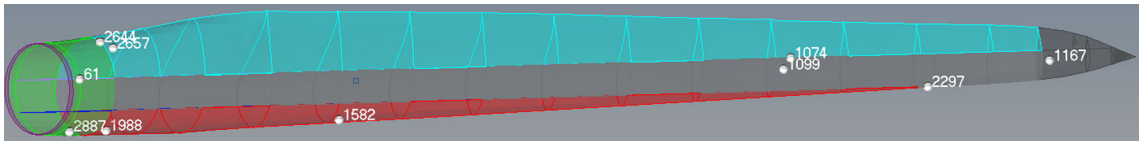

Fig. 10 Nodal locations of the 10 hotspots in RBDO

constraints even though some of them are not active anymore. Thus, there are ten hotspots after the fourth RBDO iteration. The nodal locations of the ten hotspots are shown in Fig. 10. The selected ten hotspots can well represent the fatigue critical areas in the blade model, so that the RBDO procedure does not require too many hotspots, which would cause computational burden. At the eighth and 12th RBDO iteration designs, hotspots are re-checked, but no new hotspot is found. The whole RBDO procedure is converged at the end of the 12th iteration because the maximum relative change of random design variables, 7.35E−4, is less than its convergence criterion, 1E−3, and the relative maximum constraint violation, 3.01E−4, is less than the same convergence criterion. In the entire RBDO process, 1151 DoE samples are used in total.

The accuracy of local D_{10} surrogate models at the RBDO optimum design is checked using another 1000 testing samples. Much like the accuracy of local surrogate models at the RBDO initial design is checked, the NRMSE of 20-year fatigue damage using another set of 1000 testing samples (see Eq. (18)) has been calculated. The maximum NRMSE corresponds to the ninth hotspot and is equal to 8.264E−4, which is smaller than 1E−3. Thus, the created surrogate models are accurate enough for reliability analysis at the RBDO optimum design.

The detailed composite laminate schedule, as well as the material cost, are not available for the NREL's design. Thus, it is difficult to compare the optimized design with the NREL's design currently. Instead, the RBDO initial design and the RBDO optimum design are compared. Table 6 compares the random design variables, normalized cost (objective function), true cost, mass, and the maximum probability of fatigue failure at the RBDO initial design and the RBDO optimum design. The maximum probability of fatigue failure at the RBDO optimum design is 2.281 %, so the target value of 2.275 % has been met with the optimization convergence tolerance. Moreover, the probability of fatigue failure has been reduced from 50.06 % at the RBDO initial design to 2.281 % at the RBDO optimum design, while the cost only increased by 3.01 %. Therefore, we can see that a reliable as well as cost effective design has been obtained in this RBDO process. In spite of the small cost increase, the mass of the RBDO optimum design is increased by 10.95 % compared to that of the RBDO initial design. The reason for the relatively large increase in mass is that the cheap but heavy composite material QQ1, which corresponds to the random design variables μ_1 - μ_6, is applied more at the RBDO optimum design than at the initial design. Meanwhile, the expensive composite material P2B, which corresponds to μ_7, is used 13.33 % less at the RBDO optimum design than at the initial design.

Table 6 Comparison of the RBDO initial design and the optimum design

	RBDO Initial Design	RBDO Optimum Design
μ_1	1.0000	1.1333
μ_2	1.0000	1.5708
μ_3	1.0000	1.8184
μ_4	1.0000	1.2990
μ_5	1.0000	1.1148
μ_6	1.0000	1.0913
μ_7	1.0000	0.8667
Normalized Cost	1.0000	1.0301
True Cost ($)	125605.49	129384.14
Mass (ton)	21.8050	24.1917
Maximum Probability of Failure (%)	50.06	2.281

The optimization histories of the normalized cost and the maximum probability of fatigue failure are plotted in Fig. 11. During the first three iterations, the normalized cost is increased while the probability of fatigue failure is significantly reduced. The reason is that a significant amount of composite materials QQ1, which corresponds to μ_1 - μ_6, is added to the blade in order to increase the fatigue resistance of the blade. There is a peak at the fourth iteration of the history of the probability of fatigue failure. At the iteration, a new hotspot is identified; it has a larger probability of fatigue failure than other hotspots. Between the fourth iteration and eighth iteration, both the normalized cost and the maximum probability of failure are reduced, which shows that the RBDO process

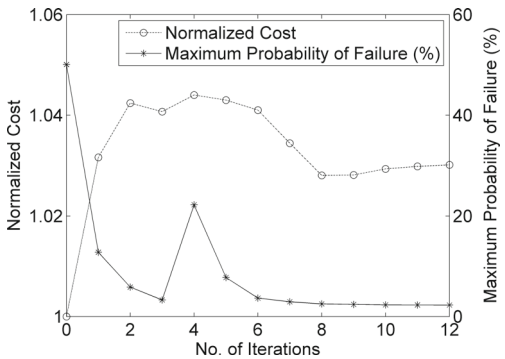

Fig. 11 Histories of normalized cost and the maximum probability of failure in RBDO

could find a more cost-effective and reliable design by tuning the seven random design variables.

8 Conclusions

A dynamic wind load uncertainty model that represents realistic wind load variability for fatigue reliability of wind turbine systems has been developed based on measured wind data. The dynamic wind load uncertainty model involves both the annual wind load variation and the wind load variation in a large spatiotemporal range. The annual wind load variation is represented by the joint probability density function (PDF) of V_{10} and I_{10}. The wind load variation in a large spatiotemporal range is represented by the PDFs of five parameters C, k, a, b, and τ, which determine the joint PDF of V_{10} and I_{10}. The best fit distribution types and parameters of the joint PDF for V_{10} and I_{10} and distributions of C, k, a, b, and τ are identified using MLE method and the 249 groups of measured wind data.

The reliability analysis method for fatigue life of the realistic and detailed composite wind turbine blade under wind load uncertainty is proposed using the sampling-based reliability analysis method. The 20-year fatigue damage is derived using Riemann integration, the wind load probability table, and the 10-min fatigue damage table. The MCS method simulates uncertain wind load using the developed dynamic wind load uncertainty model. Using the 20-year fatigue damage and simulated uncertain wind load, the probability of fatigue failure in 20 years of fatigue lifespan is estimated. In addition, RBDO is performed using the probability of fatigue failure as probabilistic constraints.

Based on the dynamic wind load uncertainty model, a mean wind load is generated to use for the DDO of the composite wind turbine blade. Using the mean wind load, deterministic 20-year fatigue damages at blade node-section points are calculated and used as DDO constraints. By fine-tuning the laminate thickness design variables, a DDO optimum design is successfully obtained through the DDO procedure. At the DDO optimum design, the fatigue life of the blade model is increased 50,000 times compared to that of the initial design, while the cost is increased only 31.53 %.

Finally, the RBDO procedure for composite wind turbine blades considering both wind load uncertainty and manufacturing variability is developed. The developed dynamic wind load uncertainty model provides realistic uncertain wind load through the designed 20-year lifespan. The RBDO objective function is normalized cost, and the probabilistic constraints are probability of fatigue failure at the selected hotspots. During the RBDO iterations, local surrogate models of 10-min fatigue damages are created to calculate 20-year fatigue damage efficiently and accurately. Using the surrogate models, probability of fatigue failure is calculated. The obtained RBDO optimum design reduces the maximum probability of fatigue failure from 50.06 % at the RBDO initial design to 2.281 % at the optimum design. This research demonstrates that applying RBDO methods to wind turbine blades could provide reliable and yet economical designs considering wind load uncertainty as well as manufacturing variability. The developed dynamic wind load uncertainty model, the reliability analysis method, the DDO procedure, and the RBDO methods could be applicable to other wind turbine components, such as the rotor hub, gears, and bearings.

The limitation of the current research is limited number of wind data. Even though 249 groups of measured wind data are used, it is desirable to collect more wind data to generate truly realistic wind load uncertainty. Another limitation of the current research is that the paper did not consider the blade deflection and blade pitch controls while wind-blade aerodynamic analysis is carried out. To include these kinds of effects, more significant wind-blade aerodynamic analysis is required, which will require high performance computing (HPC) facility. However, the proposed process in this paper should be readily extendable to apply to real wind blade RBDO designs once proper resource, including HPC facility, is available.

Acknowledgments This work is primarily supported by the Iowa Alliance Wind Innovation and Novel Development (IAWIND) 09-IPF-15 and by the National Science Foundation Experimental Program to Stimulate Competitive Research (EPSCoR) under Grant Number EPS-1101284. Any opinions, findings, and conclusions or recommendations expressed in this work are those of the authors and do not necessarily reflect the views of the National Science Foundation.

References

Burton T, Jenkins N, Sharpe D, Bossanyi E (2011) Wind energy handbook, 2nd edn. Wiley, West Sussex

Carta JA, Ramirez P, Velazquez S (2009) A review of wind speed probability distributions used in wind energy analysis case studies in the Canary Islands. Renew Sust Energ Rev 13(5):933–955

Cheng PW (2002) A reliability based design methodology for extreme responses of offshore wind turbines. Ph.D. dissertation. Wind Energy Research Institute, Delft University of Technology, Netherlands

Cho H, Choi KK, Lee I, Lamb D (2016) Design sensitivity method for sampling-based RBDO with varying standard deviation. J Mech Des 138(1):011405, http://doi.org/10.1115/1.4031829

Ditlevsen O, Madsen HO (1996) Structural reliability methods. Wiley, Chichester

Echavarria E, Hahn B, van Bussel GJW, Tomiyama T (2008) Reliability of wind turbine technology through time. J Sol Energy Eng 130: 031005

Germanischer Lloyd (2010) Guideline for the certification of wind turbines edition 2010. Hamburg, Germany

Griffith DT, Ashwill TD (2011) The Sandia 100-meter all-glass baseline wind turbine blade: SNL 100–00. SANDIA REPORT SAND2011-3779, Sandia National Laboratories, Albuquerque

Gurit (2015) Wind energy handbook. URL: http://www.gurit.com/wind-energy-handbook.aspx

Haldar A, Mahadevan S (2000) Probability, reliability and statistical methods in engineering design. Wiley, New York

Hohenbichler M, Rackwitz R (1988) Improvement of second-order reliability estimates by importance sampling. J Eng Mech 114(12): 2195–2199

Hu W, Choi KK, Gaul NJ, Cho H, Zhupanska O (2012) Reliability analysis of wind turbine blades for fatigue life under wind load uncertainty. 14th AIAA/ISSMO Multidisciplinary Analysis and Optimization Conference, Indianapolis

Hu W, Choi KK, Zhupanska O, Buchholz J (2015) Integrating variable wind load, aerodynamic, and structural analyses towards accurate fatigue life prediction in composite wind turbine blades. Struc Multidiscip Optim. doi:10.1007/s00158-015-1338-5

Institut für Solare Energieversorgungstechnik (2006) Wind Energy Report Germany 2006. ISET, Kassel

International Electrotechnical Commission (2005) Wind turbines – part I: design requirements. IEC standard, 61400–1 Third Edition

Jonkman J, Butterfield S, Musial W, Scott G (2009) Definition of a 5-MW reference wind turbine for offshore system development. NREL/TP-500-38060, National Renewable Energy Laboratory, Golden

Kong C, Bang J, Sugiyama Y (2005) Structural investigation of composite wind turbine blade considering various load cases and fatigue life. Energy 30:2101–2114

Kong C, Kim T, Han D, Sugiyama Y (2006) Investigation of fatigue life for a medium scale composite wind turbine blade. Int J Fatigue 28:1382–1388

Kyriakidis PC, Goodchild MF (2006) On the prediction error variance of three common spatial interpolation schemes. Int J Geogr Inf Sci 20(8):823–855

Mandell JF, Samborsky DD (2014) SNL/MSU/DOE Composite material fatigue database mechanical properties of composite materials for wind turbine blades version 23.0. Montana State University, Bozeman

Manuel L, Veers PS, Winterstein SR (2001) Parametric models for estimating wind turbine fatigue loads for design. Proceedings of 2001 ASME Wind Energy Symposium, 39th AIAA Aerospace Sciences Meeting & Exhibit, Reno

Manwell JF, Mcgowan JG, Rogers AL (2009) Wind energy explained: theory, design and application 2nd edition. Wiley, West Sussex

Matlab 2012a (2012) Matlab help. The MathWorks, Inc

Moriarty PJ, Holley WE, Butterfield SP (2004) Extrapolation of extreme and fatigue loads using probabilistic methods. NREL/TP-500-34421, National Renewable Energy Laboratory, Golden

Rademakers L, Braam H, Brinkman H, Ham K, Verheij F, Cleijine H, Folkerts L (2002) Handboek Risicozonering Windturbines. NOVEM, 1.1 edition

Ronold KO, Christensen CJ (2001) Optimization of a design code for wind-turbine rotor blades in fatigue. Eng Struct 23(8):993–1004

Ronold KO, Larsen GC (2000) Reliability-based design of wind-turbine rotor blades against failure in ultimate loading. Eng Struct 22(6): 565–574

Ronold KO, Jakob WH, Christensen CJ (1999) Reliability-based fatigue design of wind-turbine rotor blades. Eng Struct 21(12):1101–1114

Shokrieh MM, Rafiee R (2006) Simulation of fatigue failure in a full composite wind turbine blade. Compos Struct 74:332–342

Sutherland JH, Veers PS (1995) Fatigue case study and reliability analyses for wind turbines. ASME/JSME/JSES International Solar Energy Conference, Sandia National Laboratory, Albuquerque

Tarp-Johansen NJ (2003) Examples of fatigue lifetime and reliability evaluation of larger wind turbine components. Report No.: Risø-R-1418(EN), Risø National Laboratory, Denmark

Taylor ME (2006) Measure theory and integration. American Mathematical Society, Rhode Island

Toft HS, Sørensen JD (2011) Reliability-based design of wind turbine blades. Struct Saf 33(6):333–342

Veers PS, Winterstein SR (1997) Application of measured loads to wind turbine fatigue and reliability analysis. Proceedings of 1997 ASME Wind Energy Symposium, 35th AIAA Aerospace Science Meeting & Exhibit, Reno

TPI Composites (2003) Innovative design approaches for large wind turbine blades. Sandia Report SAND2003-0723, Sandia National Laboratory, Albuquerque

Veldkamp D (2008) A probabilistic evaluation of wind turbine fatigue design rules. Wind Energy 11:655–672

Zhao L, Choi KK, Lee I (2011) Metamodeling method using dynamic Kriging for design optimization. AIAA J 49(9):2034–2046